Electronic Supplementary Material (ESI) for ChemComm.

Hybrid Nanoarray of Cu-MOFs@H-substituted Graphdiyne with Variable Lewis Acidity for Nitrate Electroreduction

Jiahao Ma, [ab] *Ru Wang,*[b] *Biwen Wang,*[c] *Jiaxin Luo,*[d] *Qiuyu Zhang**[b] *and Sifei Zhuo**[ab]

[a.] Research&Development Institute of Northwestern Polytechnical University in Shenzhen, ShenZhen City, 518063, P. R. China.

[b.] School of Chemistry and Chemical Engineering, Xi'an Key Laboratory of Functional Organic Porous Materials, Northwestern Polytechnical University, Xi'an 710072, P. R. China.

[c.] School of Materials Science and Engineering, Northwestern Polytechnical University, Xi'an 710072, P. R. China.

[d.] Queen Mary University of London Engineering School, Northwestern Polytechnical University, Xi'an 710072, P. R. China.

1. Experimental Procedures

1.1 Chemical reagents:

Benzene-1,3,5-tricarboxylic acid (H_3BTC, 98%), 1,4-benzene- dicarboxylic (H_2BDC, ⩾99%), 2-aminoterephthalic acid ($C_8H_7NO_4$, 98%), N,N-Dimethylformamide (DMF), sodium sulfate (Na_2SO_4, ⩾99.0%), sodium hydroxide (NaOH, 97%) potassium nitrate (KNO_3,⩾99%), deuterium oxide (D_2O, 99.9 atom% D), ammonium sulfate-$^{15}N_2$ ($(^{15}NH_4)_2SO_4$, 99 atom%), sodium nitrate-^{15}N ($Na^{15}NO_3$, 99 atom%), maleic acid ($C_4H_4O_4$,⩾99.0%), triethylamine ($C_6H_{15}N$, 99%), tetrahydrofuran (C_4H_8O, 99%), 1,3,5-triethynylbenzene ($C_{12}H_6$,⩾98%), copper iodide (CuI, ⩾99.5%), bis(triphenylphosphine)palladium dichloride ($Pd(PPh_3)_2Cl_2$, Pd 15.2%), acetone (CH_3COCH_3, ⩾99.9%), ethanol (CH_3CH_2OH, ⩾99.8%) were purchased from Aladdin Chemical reagent Co., Ltd. (Shanghai, China). All chemicals are analytical grade and used as received without further purification.

1.2 Synthesis of $Cu(OH)_2$ nanorod arrays

A piece of copper foam (2×3 cm^2) was pretreated with HCl solution, acetone and deionized water to remove the organic contaminant and oxide layers. Then the copper foam was suspended in a 60 mL aqueous solution containing 0.16 mol NaOH and 8 mmol $(NH_4)_2S_2O_8$. After 14.5 min, the copper foam was taken out and washed with water and ethanol, respectively. After drying, $Cu(OH)_2$ 1D nanoarrays were obtained.

1.3 Synthesis of $Cu(OH)_2$@HsGDY nanoarrays

$Cu(OH)_2$@HsGDY nanoarrays were synthesized by the in-situ growth of HsGDY coating layers on the surface of $Cu(OH)_2$ nanoarrays by cross-coupling reaction of 1,3,5-triethynylbenzene. Briefly, $Pd(PPh_3)_2Cl_2$ (16.8 mg) and CuI (4.4 mg) were dispersed in a 50 ml eggplant-shaped flask containing tetrahydrofuran (20 mL) and trimethylamine (40 mL). After bubbling with

argon at room temperature for 30 min, the $Cu(OH)_2$ nanoarrays (2×3 cm^2) was fixed in the flask and 1,3,5-triethynylbenzene (14 mg) was added. After keeping at 60 °C for 13 h under argon atmosphere and stirring, the hybrid $Cu(OH)_2$@HsGDY nanoarrays with a color of dark yellow were obtained by ultrasonication with ethanol and rinsed with hot acetone, N, N-dimethylformamide (DMF) , and ethanol in turn. All of these treatments were designed to get rid of unreacted monomers and oligomers.

1.4 Synthesis of $Cu_3(BTC)_2$@HsGDY nanoarrays

Then the hybrid $Cu(OH)_2$@HsGDY nanoarrays were worked as dual-template to evolve $Cu_3(BTC)_2$@HsGDY nanoarrays. Briefly, the $Cu(OH)_2$@HsGDY nanoarrays were fixed in a flask containing 9 mL water, 23.3 mL ethanol and 1.05 g $H_3(BTC)_2$. After setting for 6 h, $Cu_3(BTC)_2$@HsGDY nanoarrays were acquired by washing with ethanol.

1.5 Synthesis of Cu(BDC)@HsGDY nanoarrays

The conversion of $Cu(OH)_2$@HsGDY nanoarrays to Cu(BDC)@HsGDY nanorod arrays were performed through a vapor-phase strategy. Briefly, 400 mg PTA and the $Cu(OH)_2$@HsGDY nanoarrays were placed in a crucible with lid. Then it was heated to 350 °C with a heating rate of 5 °C min^{-1} under Ar atmosphere. After 1 h, Cu(BDC)@HsGDY nanoarrays were fabricated after washing with ethanol.

1.6 Synthesis of Cu(BDC-NH_2)@HsGDY nanoarrays

The conversion of $Cu(OH)_2$@HsGDY nanoarrays to Cu(BDC-NH_2)@HsGDY nanoarrays were performed through a solvothermal method. Briefly, 11 mg 2-aminoterephthalic acid was dissolved into 30 mL of DMF under sonication for 5min. Then, the solution was transferred to a 50 mL autoclave containing the $Cu(OH)_2$ nanoarrays. After hydrothermal treatment at 100 °C for 48 h in an oven, Cu(BDC-NH_2)@HsGDY nanoarrays were fabricated. Before electrochemical

texted, the Cu(BDC-NH_2)@HsGDY nanoarrays were activated in a vacuum oven at 170 °C for 12 h to remove the coordinated DMF molecule.

1.7 Synthesis of $Cu_3(BTC)_2$, Cu(BDC) and Cu(BDC-NH_2) film

These Cu-MOFs were fabricated through a similar method by replacing $Cu(OH)_2$@HsGDY nanoarrays with $Cu(OH)_2$ nanoarrays. The only difference is the reaction time. The conversion of $Cu(OH)_2$ nanoarrays to $Cu_3(BTC)_2$ film was decreased to 1 h. The conversion of $Cu(OH)_2$ nanoarrays to Cu(BDC-NH_2) film was reduced to 24 h.

1.8 Synthesis of HsGDY nanotube arrays

The HsGDY nanotube arrays were synthesized by immersing $Cu(OH)_2$@HsGDY nanorod arrays into a 3 M HCl solution. After 10 min, the HsGDY nanotube arrays were obtained.

1.9 Electrochemical measurements

The electroreduction of nitrate was carried out in a two-compartment cell separated with a Nafion film. The Pt piece, Ag | AgCl (Saturated KCl) electrode and the catalysts/CF (1×1 cm^2) were served as the counter electrode, reference electrode, and working electrode, respectively. The cathode chamber includes 0.5 M Na_2SO_4 + 200 ppm KNO_3 solution (45 ml), while only 0.5 M Na_2SO_4 solution in the anode chamber. Before test, to get rid of the dissolved N_2, Ar (99.99% purity) gas was bubbled in the cathode chamber for 15 min. The LSV was conducted at a scan rate of 10 mV s^{-1}. The potentiostatic test was performed from -0.5 ~ -0.9 V vs. RHE for 2 h at a stirring rate of ~400 rpm. The NO_3^- and the produced NO_2^- and NH_3 are quantified based on the standard method by using UV-Vis spectrophotometry.[1] The UV-Vis absorption spectra and the corresponding calibration curves are shown in Figure S18-20. ^{15}N Isotope Labeling Experiments were carried out to eliminate the influence of dissolved N_2 based on reported methods.[2]

1.10 Characterization

SEM images were taken with a FEI microscope operated at 10 kV. TEM and HRTEM analyses were obtained with a FEI Themis Z microscope operated at 200 kV. XRD patterns of the samples were recorded with a Bruker diffractometer using Cu Kα radiation. The ultraviolet-visible (UV-Vis) absorbance spectra were collected on a PerkinElmer LAMBDA 365 spectrophotometer. Raman spectra was measured on a Alpha300R with a 473 nm laser wavelength excitation and spectra were up to 3000 cm^{-1}. XPS was taken with on an Axis Supra instrument to detect the surface elemental composition and the chemical states of the samples. BET was recorded on a BELSORP-MAX instrument to analyze the surface area and pore size distributions of the synthesized materials. The Fourier transform infrared spectroscopy (FTIR) was recorded on a Bruker Tensor II spectrometer.

1.11 Calculation of the yield, selectivity and Current efficiency

The NH_3 Faradaic efficiency was calculated based on the total charge transferred through the electrode and the charge used to product the N-NH_3 using Equation (1):

$$NH_3\ Faradaic\ efficiency = (8F \times c_{N\text{-}NH3} \times V) / (M_{N\text{-}NH3} \times Q) \quad [1]$$

Where $c_{N\text{-}NH3}$ is the concentration of N-NH_3 after the electrochemical test, $M_{N\text{-}NH3}$ represents the molar mass of N-NH_3, V is the volume of electrolyte, F is the Faradaic constant (96485 C mol^{-1}) and Q is the total charge passing the electrode.

The yield of $NH_{3(aq)}$ was calculated using Equation (2):

$$NH_3\ Yield = (c_{N\text{-}NH3} \times V) / (M_{N\text{-}NH3} \times t \times A) \quad [2]$$

Where A is the area of the working electrode.

The selectivity of $NH_{3(aq)}$ was calculated using Equation (3):

$$NH_3\ Selectivity = \square c_{N\text{-}NH3} / c_{N\text{-}NO3^-} \times 100\% \quad [3]$$

Where $c_{N\text{-}NO_3^-}$ represents the concentration difference of N-NO_3^- before and after electrolysis, $c_{N\text{-}NH_3}$ is the generated concentration of N-NH_3.

The NO_3^- conversion rate was calculated using Equation (4):

$$NO_3^- \text{ conversion} = c_{N\text{-}NO_3^-} / c_0 \times 100\% \quad [4]$$

Where c_0 represents the initial concentration (200 ppm) of nitrate in electrolyte.

1.12 Determination of products

The concentrations of NO_3^-, NH_3 and NO_2^- were determined by using UV-vis spectrophotometry according to the following standard method:

Determination of NO_3^-: In detail, a certain volume of electrolyte was taken out after electroreduction process and diluted with deionized water to 5 ml to the detection range. Then, 100 μL HCl solution (1 M) and 10 μL 0.8 wt % sulfamic acid aqueous solution were added. The absorbance at 200 and 275 nm were recorded using an ultraviolet–visible spectroscopy. The final absorbance value was calculated using the equation: $A = A_{220\ nm} - 2A_{275\ nm}$. The standard concentration-absorbance curve was calibrated by a series of standard sodium nitrate solutions.

Determination of NH_3: Ammonia-N in the aqueous solution was determined using Nessler's reagent as the color reagent. Firstly, a certain volume of electrolyte was diluted to 5 mL to the detection range. Next, 0.1 mL potassium sodium tartrate solution (ρ= 500 $g \cdot L^{-1}$) and 0.1 ml Nessler's reagent was added into the above diluted electrolyte. The absorbance intensity at the wavelength of 420 nm was recorded after fully mixing and sitting for 20 minutes. The concentration was calculated by standard concentration-absorbance curve.

Determination of NO_2^-: The color reagent was obtained by dissolving N-(1-Naphthyl) ethylenediamine dihydrochloride (0.2 g), p-aminobenzene sulfonamide (4 g) and phosphoric acid (10 mL, ρ= 1.70 g/mL) in 50 mL deionized water. A certain volume of electrolyte was diluted to

5 mL to the detection range. Then, 0.1 ml of the color reagent was added into the above solution. After stirring for 20 min, the absorbance intensity at a wavelength of 540 nm was recorded.

To minimize the experimental error, all the experimental data were recorded by averaging the testing values after three repeated times. The error bar of each data point was obtained from the standard deviation of multiple measurement on different set of samples.

1.13 ^{15}N isotope-labeling experiment

The isotopic labeling nitrate reduction experiments were carried out using 99.21% $Na^{15}NO_3$ as the feeding N-source to clarify the source of ammonia. Firstly, 45 mL solution containing 200 ppm $Na^{15}NO_3$ + 0.5 M Na_2SO_4 was used as the electrolyte. After electroreduction, the pH value of the final electrolyte was adjusted to be weak acid with 0.5 M H_2SO_4. Next, 0.015g maleic acid (600 ppm) was added into 25 mL of the abovementioned solution as external standards. Finally, 50 μL deuterium oxide (D_2O) was added in 0.5 mL of the abovementioned solution for the NMR detection (^{1}H NMR, 400 MHz). The calibration curve was created by using a series of $^{15}NH_4^+$-^{15}N solutions(($(^{15}NH_4)_2SO_4$)) with known concentration (50, 100, 150, 200, 250 ppm).

1.14 Preparation of MOFs-acetone

The MOFs-acetone were prepared according to a literature method.[3] Briefly, the activated Cu-MOFs were immersed in acetone under Ar for 1h. Next, the acetone-exchanged samples were collected by filtration and dried in air. Then, the MOFs-acetone samples were fabricated by evacuating the acetone-exchanged samples for 2h.

2. Supplementary Figures and Tables

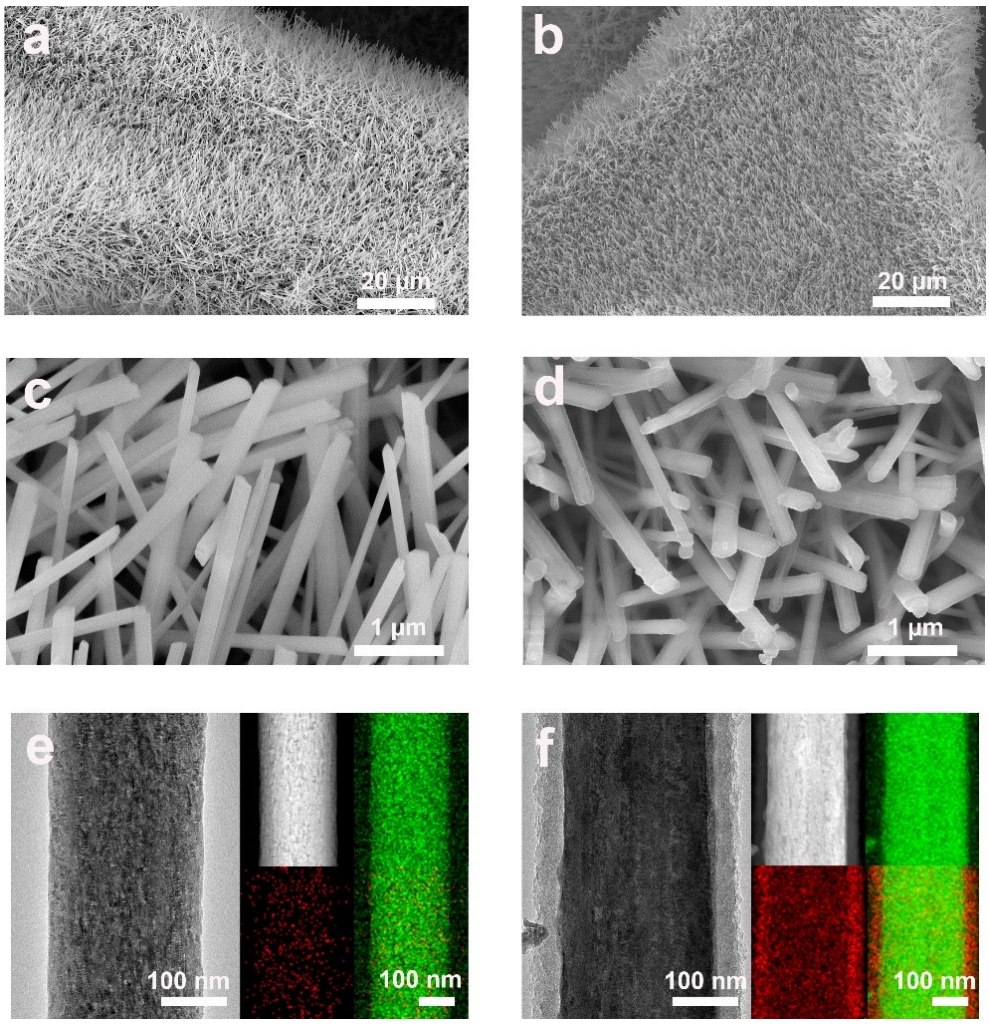

Figure S1 (a,c,e) SEM, TEM and STEM-EDS mapping of $Cu(OH)_2$ nanoarrys, (b,d,f) SEM, TEM and STEM-EDS mapping of $Cu(OH)_2$@HsGDY nanoarrys (green: Cu, red: carbon).

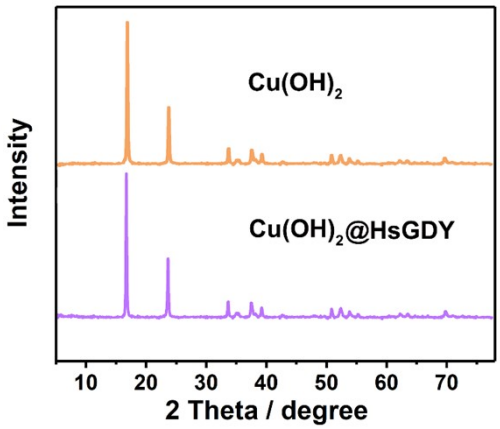

Figure S2. XRD patterns of $Cu(OH)_2$ nanoarrays before and after HsGDY coating.

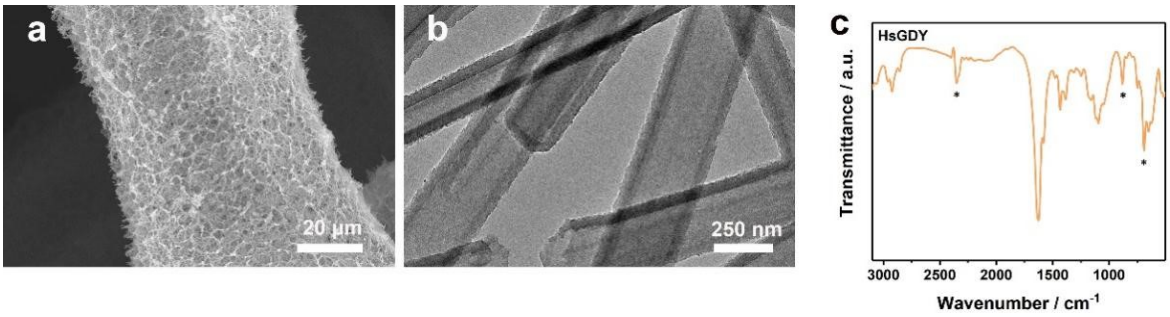

Figure S3 (a-c) SEM image, TEM images and FTIR spectrum of the HsGDY nanoarrays after removing the $Cu(OH)_2$ cores by acid. The representative vibration peaks for C≡C bond (2332 cm^{-1}) and aromatic C-H (877 cm^{-1}, 688 cm^{-1}) identify the structure of HsGDY with sp- and sp^2-hybridized carbon atoms.[4]

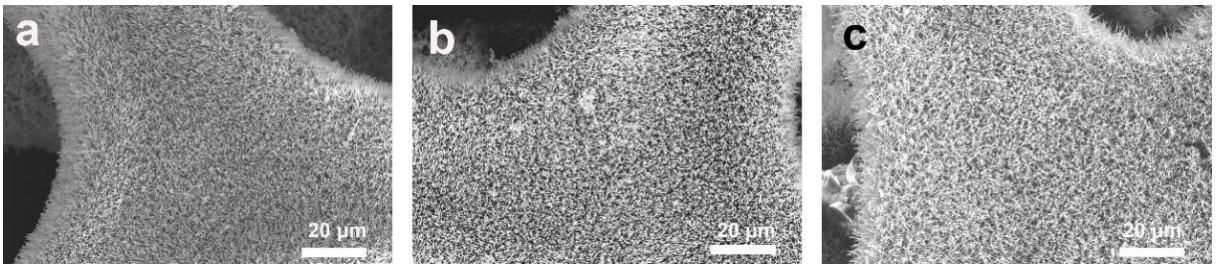

Figure S4 (a-c) SEM images of $Cu_3(BTC)_2$@HsGDY nanoarrys (a), Cu(BDC)@HsGDY nanoarrys (b) and Cu(BDC-NH_2)@HsGDY nanoarrys (c).

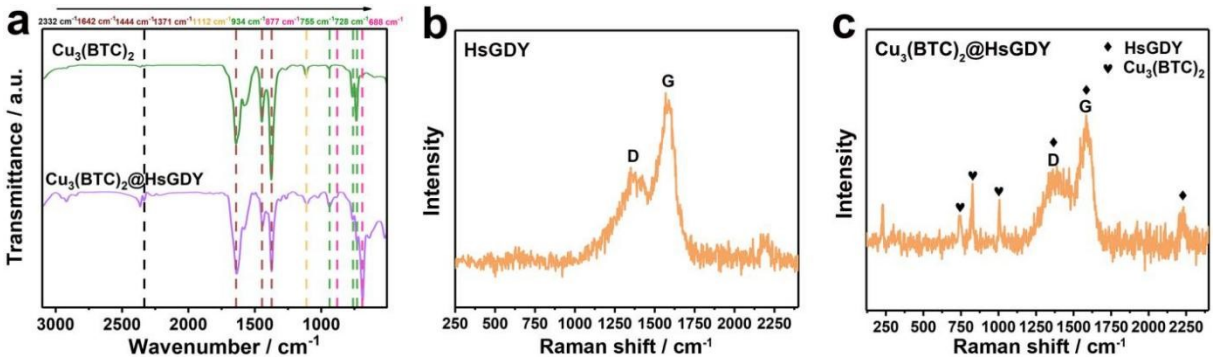

Figure S5 a) FTIR spectra of $Cu_3(BTC)_2$ and $Cu_3(BTC)_2$@HsGDY nanoarrays; b-c) Raman spectra of HsGDY (b) and $Cu_3(BTC)_2$@HsGDY (c). In details, the peaks assigned to the $Cu_3(BTC)_2$ are as follows: 934, 755, 728 cm^{-1}: C–CO2 stretching, 1112 cm^{-1}: C–O stretching, 1642, 1444, 1371 cm^{-1}: COO–Cu2 stretching.[5] The floowing peaks belong to HsGDY: 2332 cm^{-1}: C≡C bond, 877 cm^{-1}, 688 cm^{-1}: aromatic C-H.

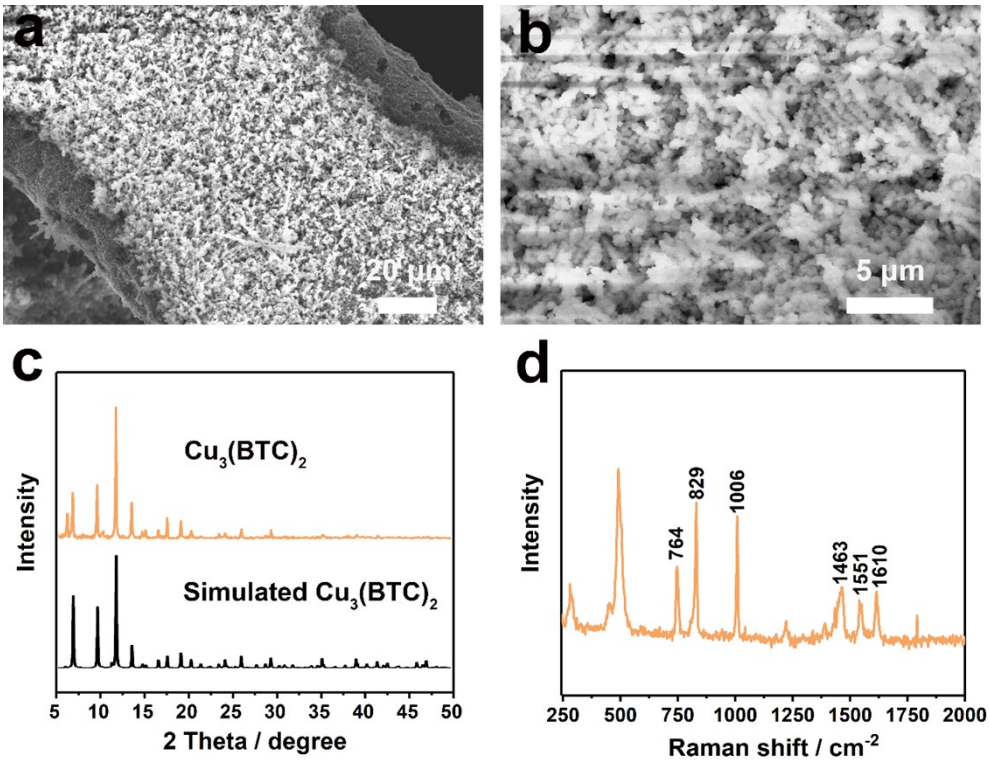

Figure S6 (a-d) SEM images (a,b), XRD patterns (c), and Raman spectrum (d) of $Cu_3(BTC)_2$. As shown in the SEM images, some chain-like $Cu_3(BTC)_2$ nanoarrays with brittle joinpoints are obtained, which distinguish from $Cu_3(BTC)_2$@HsGDY nanoarrays with homogeneous $Cu_3(BTC)_2$ along with HsGDY. Its XRD pattern fit well the simulated $Cu_3(BTC)_2$ data with face-centered cubic structure. The peaks of 746 cm^{-1}, 829 cm^{-1} shown in the Raman spectrum correspond to out-of-plane ring bending vibrations and out-of-plane ring (C–H) bending modes. The peaks located at 1006 cm^{-1} and 1610 cm^{-1} can be assigned to C=C stretching modes of the benzene ring, while the ones at 1463 cm^{-1} and 1551 cm^{-1} are associated with the symmetric and asymmetric stretching of the carboxylate units.

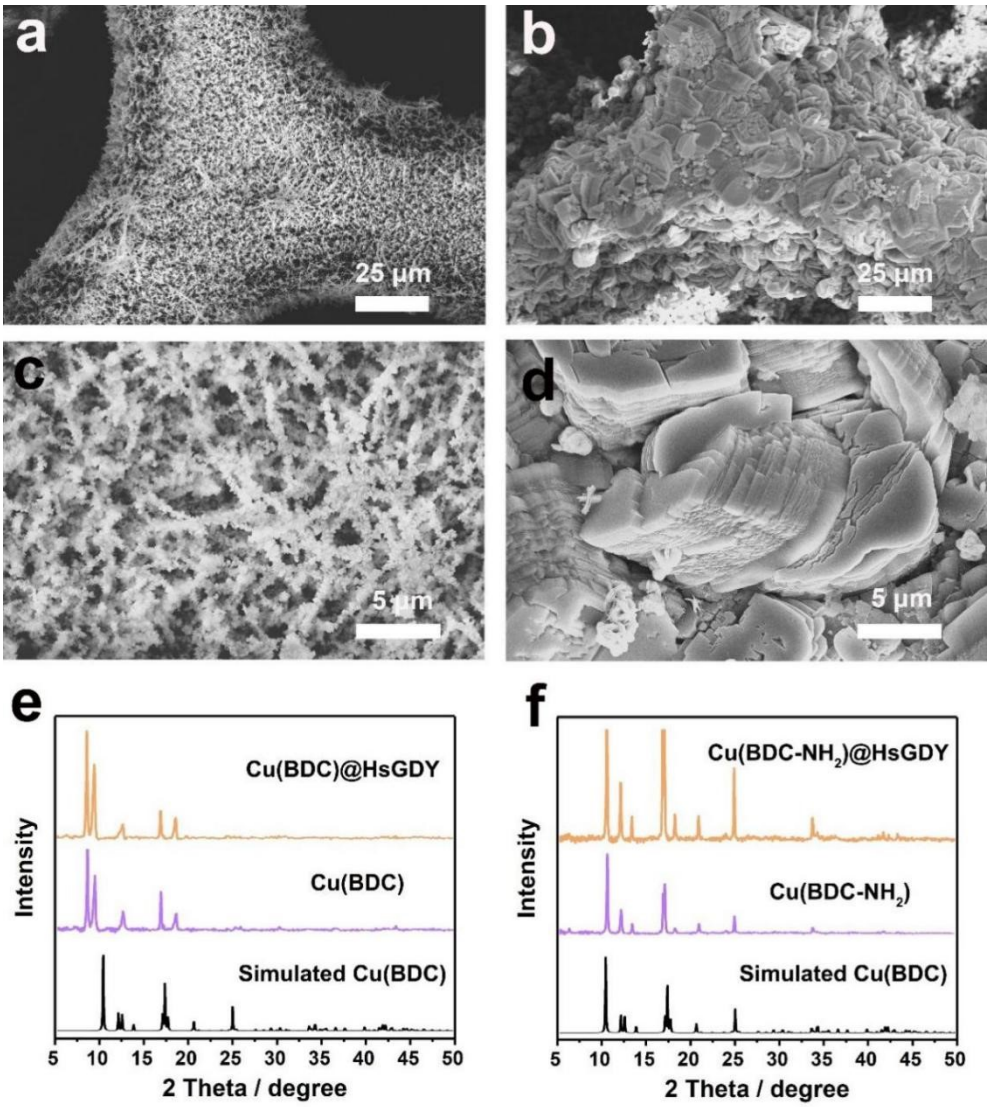

Figure S7 (a-d) SEM images of Cu(BDC) (a,c) and Cu(BDC-NH_2) (b, d), respectively. (e,f) XRD patterns of Cu(BDC) (e) and Cu(BDC-NH_2) (f), respectively. As shown in the SEM images, some chain-like Cu(BDC) nanoarrays and micro-sized Cu(BDC-NH_2) bulks losing control are prefered without HsGDY control. Notably, the Cu(BDC) and simulated Cu(BDC) demonstrate different diffraction patterns, this is attributed to the difference between the Cu(BDC)·DMF and the Cu(BDC) without coordination with DMF fabricated by the solvent-free process.[6,7] The XRD patterns of Cu(BDC-NH_2) and Cu(BDC-NH_2)@HsGDY fit well with that

of simulated Cu(BDC), indicating the similar crystalline structure of Cu(BDC) and Cu(BDC-NH_2) with monoclinic crystal structure.

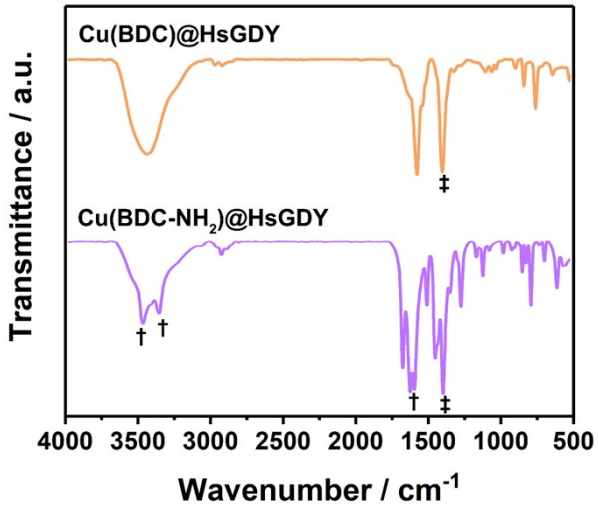

Figure S8 FTIR spectra of Cu(BDC)@HsGDY and Cu(BDC-NH_2)@HsGDY nanoarrays. The strong peaks at 1390 cm^{-1} is corresponds to symmetric vibrations of carboxylate anions, while double peaks at 3476 and 3364 cm^{-1} and the strong peak at 1609 cm^{-1} correspond to the -NH_2 stretching vibration and the N-H bending vibration respectively.[8,9]

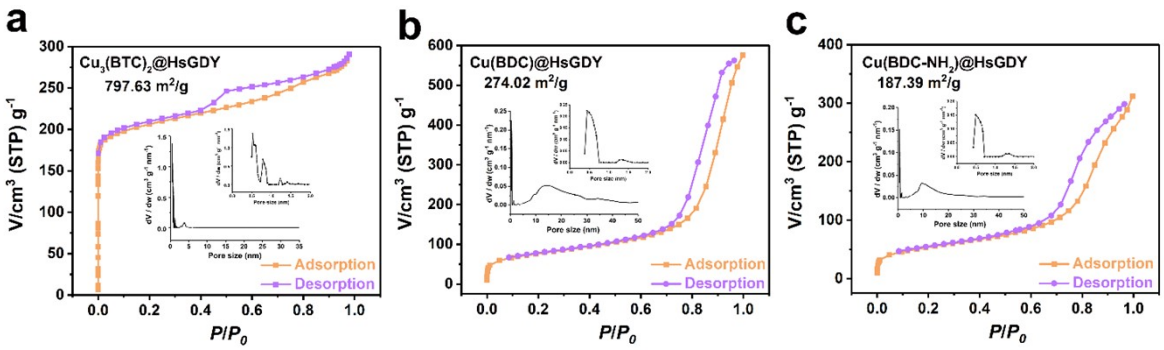

Figure S9 N_2 adsorption/desorption isotherms of the as-prepared Cu-MOFs@HsGDY nanohybrids. The inset image is the corresponding pore size distribution diagram. As a result, all of the three Cu-MOFs@HsGDY have not only micropores of HsGDY (1.3 nm) and Cu-MOFs (0.5, 0.8 and 1.2 nm for $Cu_3(BTC)_2$@HsGDY; 0.5 nm for Cu(BDC)@HsGDY and Cu(BDC-NH_2)@HsGDY), but also mesopores distributed in the interior of Cu-MOFs.

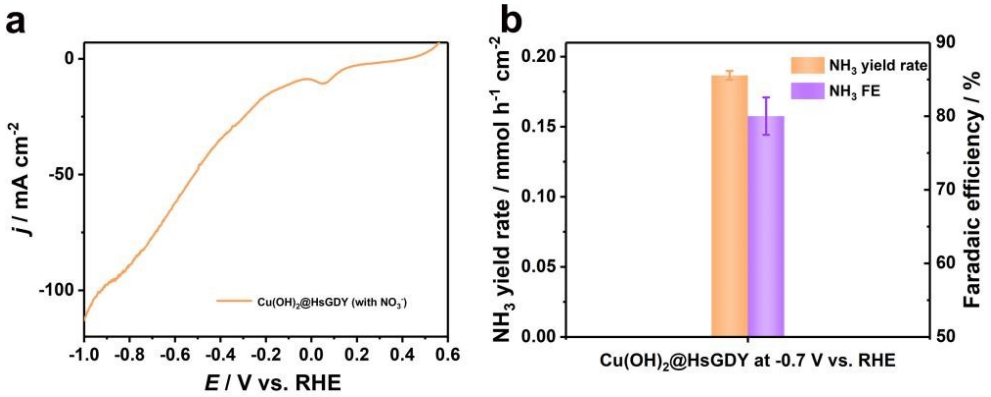

Figure S10. LSV curves of $Cu(OH)_2$@HsGDY nanoarray in 0.5 M Na_2SO_4 with 200 ppm NO_3^-. b) Yield rate and FE of $Cu(OH)_2$@HsGDY nanoarray at -0.7 V vs RHE. As a result, it delivers an ammonia yield rate of 0.186 mmol h^{-1} cm^{-2} with a FE around 80% at -0.7 V vs RHE. This value is lower than that of all of the $Cu_3(BTC)_2$@HsGDY (Y_{NH3}: 0.265 mmol h^{-1} cm^{-2}, FE: 90.2%), Cu(BDC)@HsGDY (Y_{NH3}: 0.224 mmol h^{-1} cm^{-2} , FE: 80.1%) and Cu(BDC-NH_2)@HsGDY (Y_{NH3}: 0.23 mmol h^{-1} cm^{-2} , FE: 80.3%). Therefore, it is necessary to adjust the physical and chemical environment of Cu^{2+} by transforming $Cu(OH)_2$ to Cu-MOFs with controllable Lewis acidity strength.

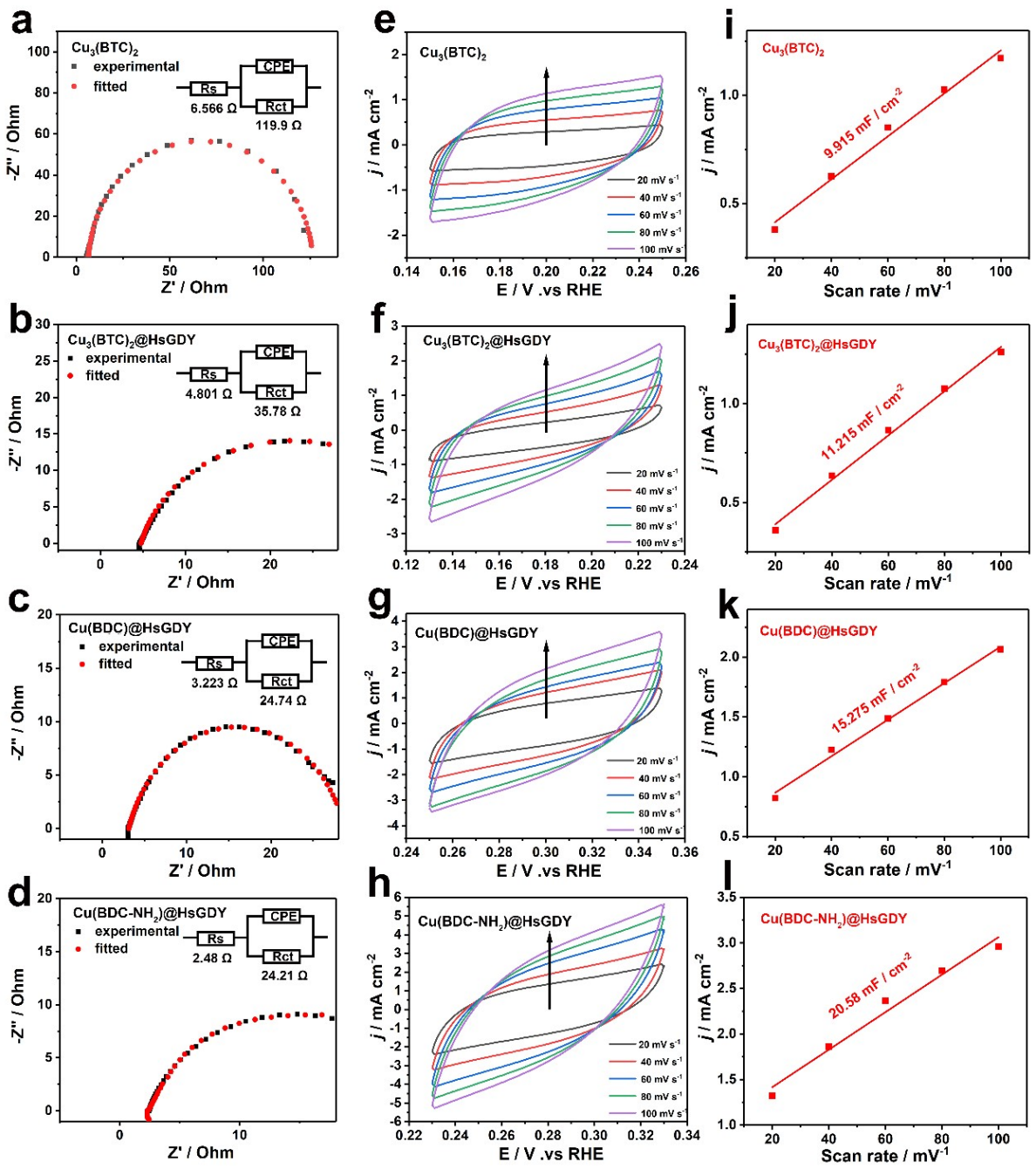

Figure S11 (a-d) EIS Nyquist plots of $Cu_3(BTC)_2$ (a), $Cu_3(BTC)_2$@HsGDY (b), Cu(BDC)@HsGDY (c), Cu(BDC-NH_2)@HsGDY (d) and their corresponding equivalent electrical circuits conducted at an overpotential of 200 mV in 0.5 M Na_2SO_4 + 200 ppm NO_3^-. (e-l) CV curves within the potential range of no faradaic reactions of $Cu_3(BTC)_2$ (e), $Cu_3(BTC)_2$@HsGDY (f), Cu(BDC)@HsGDY (g), Cu(BDC-NH_2)@HsGDY (h) and the their

corresponding electrode double-layer capacitance (C_{dl}). The specific capacitance for the flat surface was assumed as 40 μF cm^{-2} (normally 20-60 μF cm^{-2}).

$$A_{ECSA}^{Cu_3(BTC)_2} = \frac{9.915\ mF\ cm^{-2}}{40\ \mu F\ cm^{-2}\ per\ cm_{ECSA}^2} = 247.8\ cm_{ECSA}^2$$

$$A_{ECSA}^{Cu_3(BTC)_2@HsGDY\ nanoarrays} = \frac{11.215\ mF\ cm^{-2}}{40\ \mu F\ cm^{-2}\ per\ cm_{ECSA}^2} = 280.0 cm_{ECSA}^2$$

$$A_{ECSA}^{Cu(BDC)@HsGDY\ nanoarrays} = \frac{15.275\ mF\ cm^{-2}}{40\ \mu F\ cm^{-2}\ per\ cm_{ECSA}^2} = 381.8\ cm_{ECSA}^2$$

$$A_{ECSA}^{Cu(BDC-NH_2)@HsGDY\ nanoarrays} = \frac{20.580\ mF\ cm^{-2}}{40\ \mu F\ cm^{-2}\ per\ cm_{ECSA}^2} = 514.5 cm_{ECSA}^2$$

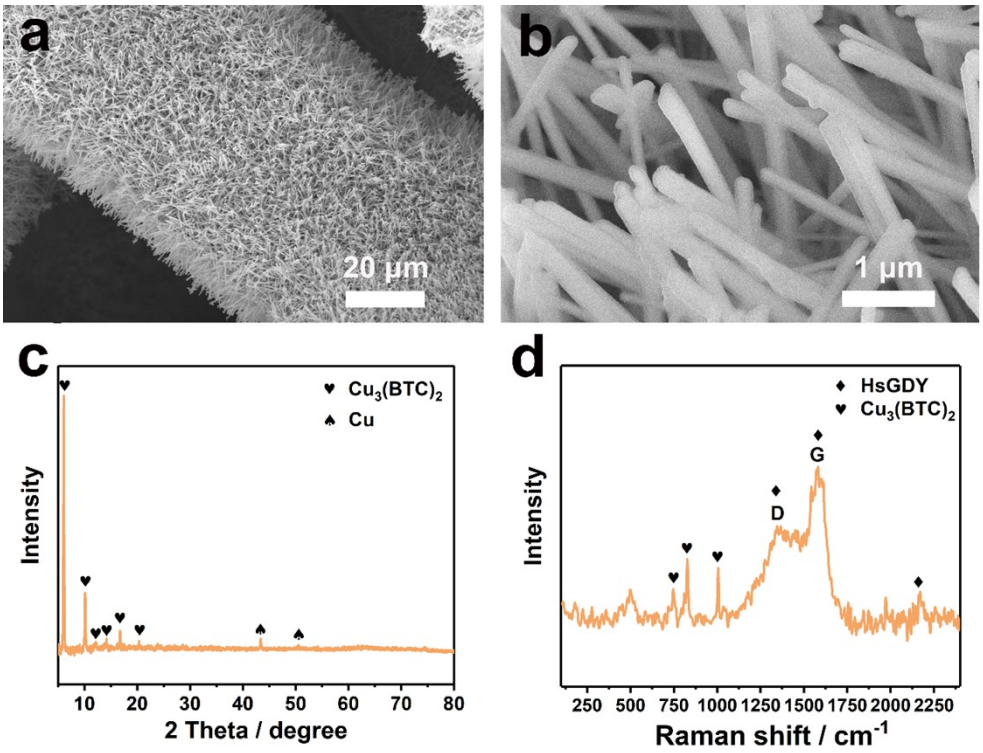

Figure S12 (a-d) SEM images (a,b), X-ray diffraction (XRD) pattern (c), and Raman spectrum (d) of $Cu_3(BTC)_2$@HsGDY after the electrochemical text. Notably, both 1D nanoarray and crystal structure of $Cu_3(BTC)_2$ in the presence of HsGDY are well preserved along with the electroreduction process.

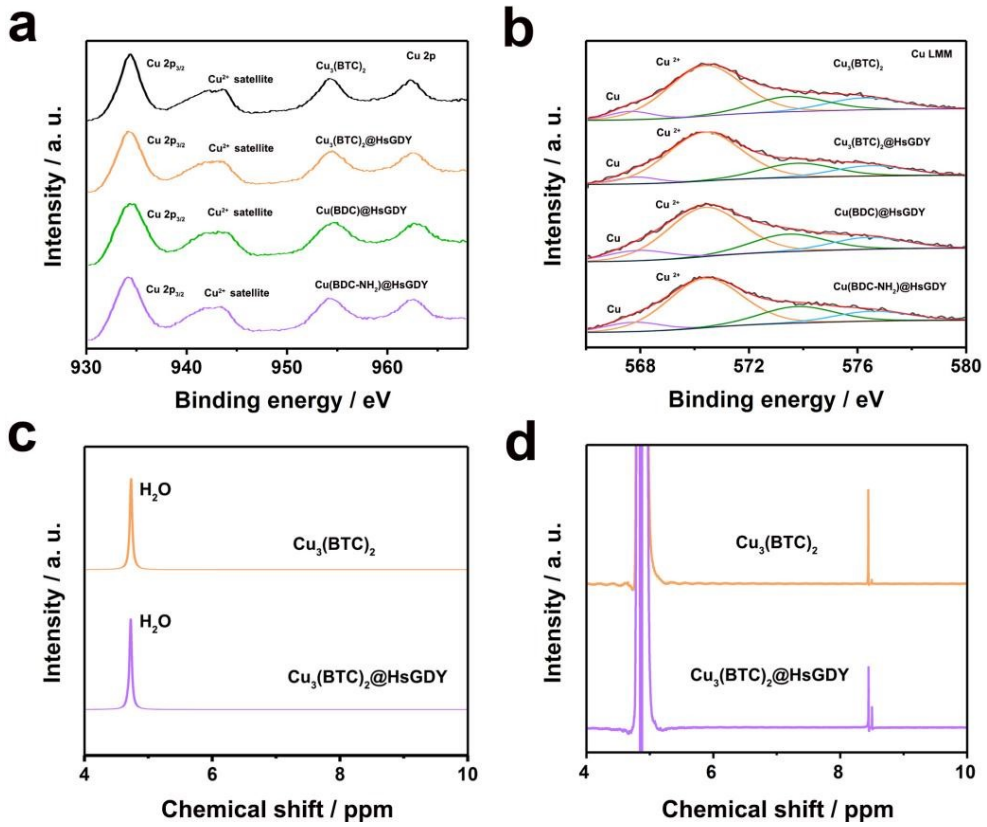

Figure S13. a,b) XPS spectra of $Cu_3(BTC)_2$, $Cu_3(BTC)_2$@HsGDY, Cu(BDC)@HsGDY and Cu(BDC-NH_2)@HsGDY after potentiostatic test at -0.7 V vs RHE for 2 hours. c,d) The leaching test of ligand by using ^1H NMR after potentiostatic test at -0.7 V vs RHE for 2 hours in 0.5 M Na_2SO_4 with 200 ppm NO_3^- (a) and 10 hours in 0.5 M Na_2SO_4 with 0.2 M NO_3^-, respectively. As a result, after etching the HsGDY coating with Ar ions, we find that the dominant state of Cu in all of the three Cu-MOFs are Cu^{2+}. Only in the Cu LMM Auger spectra, we could detect the presence of a spot of Cu with similar Cu/Cu^{2+} ration in all of the three Cu-MOFs. Besides, during the first 2 hours of potentiostatic test at -0.7 V vs RHE, we do not detect the leaching of ligand from both $Cu_3(BTC)_2$ and $Cu_3(BTC)_2$@HsGDY. However, when we prolong the potentiostatic test at -0.7 V vs RHE from 2 to 10 hours in 0.5 M Na_2SO_4 with 0.2 M NO_3^-, the characteristic peaks of BTC have been detected in the electrolyte for both $Cu_3(BTC)_2$ and $Cu_3(BTC)_2$@HsGDY. In spite of that, when we analyze the structure of $Cu_3(BTC)_2$@HsGDY

after test, both 1D nanoarray and the main crystal structure of Cu-MOFs are preserved. In contrast, the diffraction peaks of copper gradually surpass that of Cu-MOFs for $Cu_3(BTC)_2$ electrode. It means that the potential-induced redox reactions as well as the water-triggered destabilization of $Cu_3(BTC)_2$ could be inhibited in some level in the presence of HsGDY. On the one hand, the extended π-conjugated system qualify HsGDY as circular electron reservoir by shortening the diffusion path of electrons across Cu-MOFs, which minimize the hazards to the bridging sites under mild potentials. On the other, the microporous structure of HsGDY layer make it a physical membrane between Cu-MOFs and aqueous solution, which will protect Cu-MOFs from soaking in water but allow moderate water with nitrate access to Cu^{2+} sites. By reason of the foregoing, in the initial 2 hours below -0.7 V vs RHE, it is safe to compare the Lewis acid promoted effect of these Cu-MOFs toward selective ammonia electrosynthesis from nitrate.

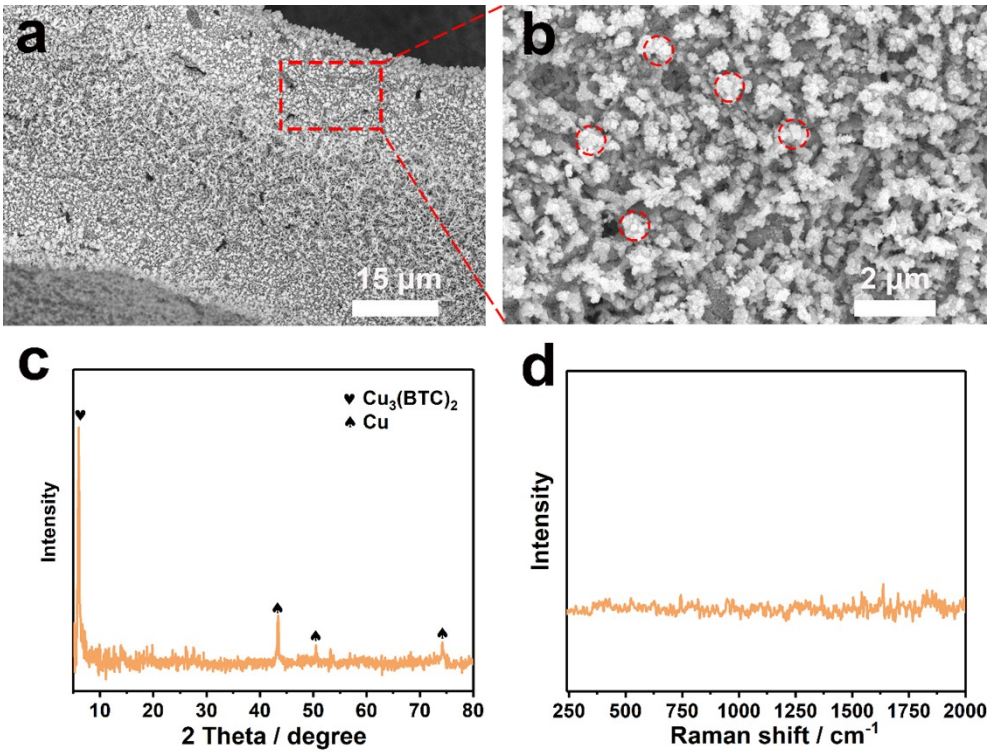

Figure S14 (a-d) SEM images (a,b), X-ray diffraction (XRD) patterns (c), and Raman spectrum (d) of $Cu_3(BTC)_2$ after the electrochemical text at -0.7 V vs RHE for 10 hours (5 cycles). However, without protection of HsGDY, the diffraction peaks of copper gradually emerge and surpass that of $Cu_3(BTC)_2$ until all it's covered.

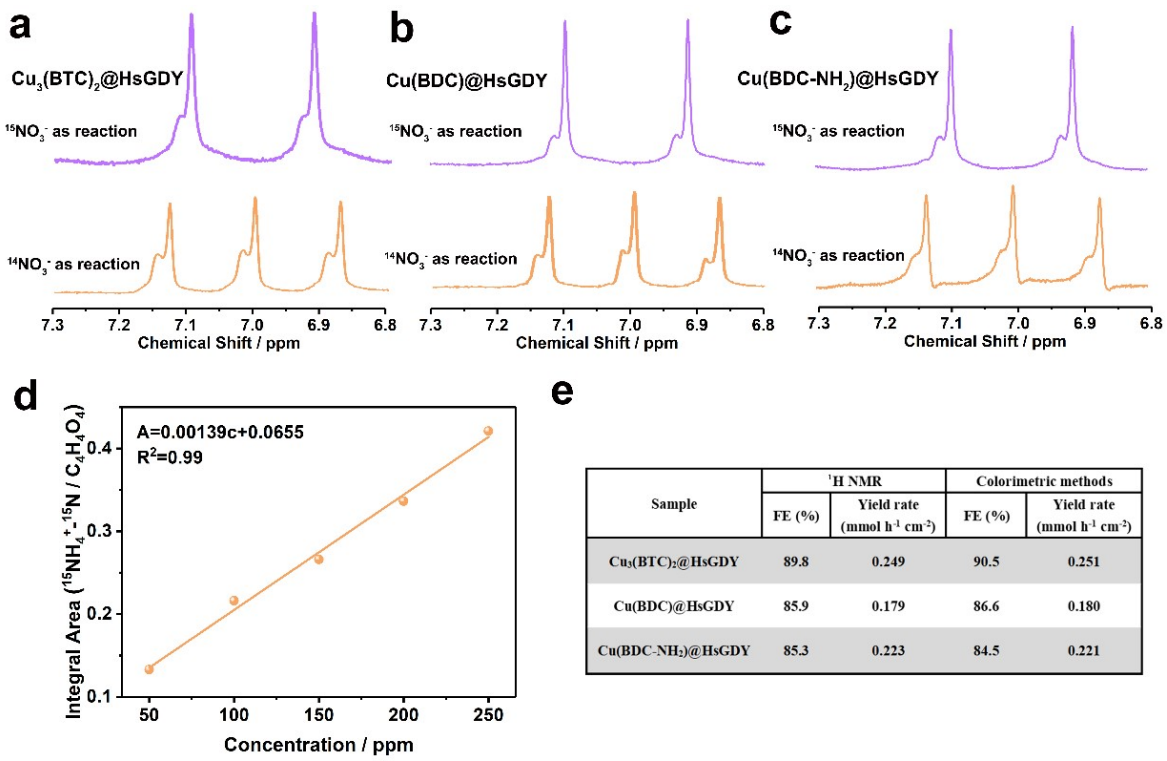

Sample	^{1}H NMR		Colorimetric methods	
	FE (%)	Yield rate (mmol h^{-1} cm^{-2})	FE (%)	Yield rate (mmol h^{-1} cm^{-2})
$Cu_3(BTC)_2$@HsGDY	89.8	0.249	90.5	0.251
Cu(BDC)@HsGDY	85.9	0.179	86.6	0.180
Cu(BDC-NH_2)@HsGDY	85.3	0.223	84.5	0.221

Figure S15 (a-c) ^{1}H NMR spectra (400 MHz) of the electrolyte after electrochemical texts by using $^{14}NO_3^-$ and $^{15}NO_3^-$ as N-source with $Cu_3(BTC)_2$@HsGDY (at -0.7 V vs. RHE for 2h) (a), Cu(BDC)@HsGDY (at -0.6 V vs. RHE for 2h) (b), Cu(BDC-NH_2)@HsGDY (at -0.6 V vs. RHE for 2h) (c), (d) The standard curve of integral area ($^{15}NH_4^+$-^{15}N/$C_4H_4O_4$) against $^{15}NH_4^+$-^{15}N concentration. (e) Comparison of the quantitative results of $^{15}NH_4^+$-^{15}N for $Cu_3(BTC)_2$@HsGDY, Cu(BDC)@HsGDY, and Cu(BDC-NH_2)@HsGDY nanoarrays obtained by different quantitative methods.

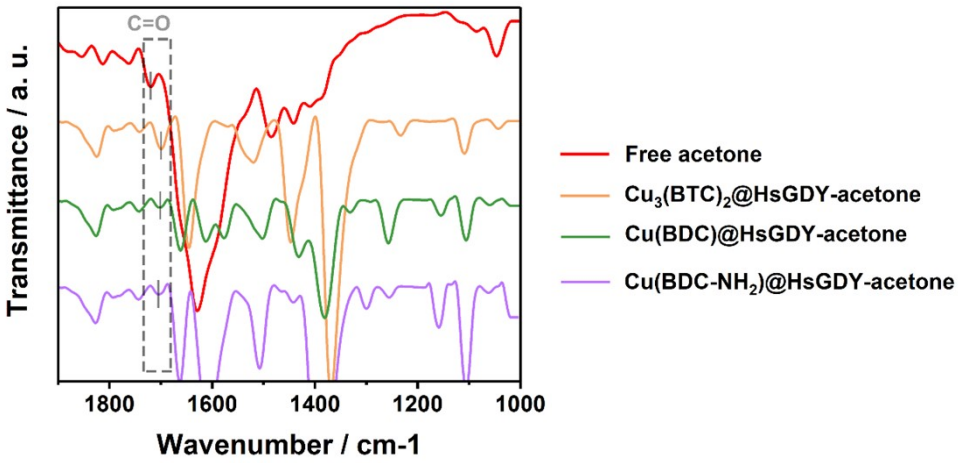

Figure S16 FTIR spectra of Cu-MOFs-acetone. Since acetone could bind to the unsaturated metal ions, which result in the elongation of C=O bond,[10,11] hence it is worked as probe molecule to verify the Lewis acidity strength of the Cu^{2+} sites in Cu-MOFs@HsGDY. Firstly, the peak around 1722.21 cm^{-1} corresponds to the C=O stretching band of free acetone, which is utilized as the reference value. Then, the C=O band position of acetone was observed at 1700.20 cm^{-1}, 1701.98 cm^{-1} and 1702.81 cm^{-1} for $Cu_3(BTC)_2$@HsGDY-acetone, Cu(BDC)@HsGDY-acetone and Cu(BDC-NH_2)@HsGDY-acetone, respectively. As a result, the Δν (C=O) value of the $Cu_3(BTC)_2$ is 22.01 cm^{-1} which is close to the previous report,[12] and it is higher than that of Cu(BDC)@HsGDY (20.23 cm^{-1}) and Cu(BDC-NH_2)@HsGDY (19.40 cm^{-1}). Thus the Lewis acidity of these MOFs follows the order of $Cu_3(BTC)_2$@HsGDY > Cu(BDC)@HsGDY > Cu(BDC-NH_2)@HsGDY.

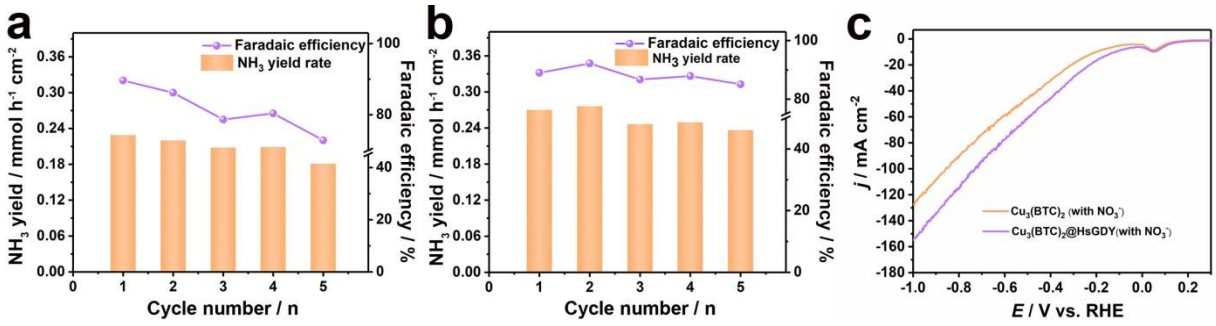

Figure S17. a,b) The consecutive recycling test of $Cu_3(BTC)_2$ (e) and $Cu_3(BTC)_2$@HsGDY (f) at -0.7 V vs RHE, respectively. c) LSV curves of $Cu_3(BTC)_2$ and $Cu_3(BTC)_2$@HsGDY after 5 cycles at -0.7 V vs RHE, respectively. As a result, after 5 potentiostatic test cycles, $Cu_3(BTC)_2$@HsGDY not only shows a higher apparent current density, but also both superior FE_{NH3} and Y_{NH3} than that of $Cu_3(BTC)_2$.

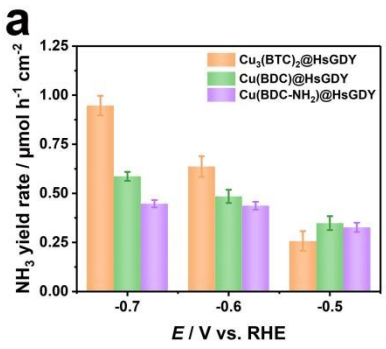

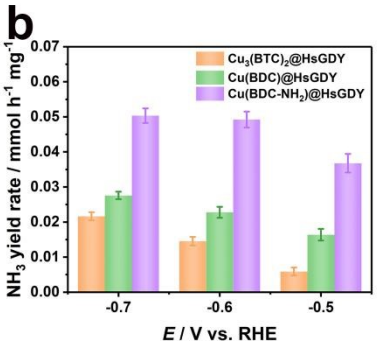

c

Sample	Cu mass per unit area (mg / cm^{-2})	Estimated catalyst mass per unit area (mg / cm^{-2})
$Cu_3(BTC)_2$@HsGDY	3.9 mg	12.3 mg
Cu (BDC)@HsGDY	2.3 mg	8.1 mg
Cu (BDC-NH_2)@HsGDY	1.2 mg	4.6 mg

Figure S18 Ammonia yield rates of these Cu-MOFs normalized by ECSA (a) and mass loading (b), respectively. Notably, no matter normalized by geometric area, ECSA or mass loading, all of the three Cu-MOFs demonstrate different Y_{NH3} at the same potentials (e.g. -0.5, -0.6 and -0.7 V vs RHE). This different structure-activity relationship at the same potential suggests that the

activity of these three Cu-MOFs originates from the Cu^{2+} sites with different coordination environments rather than the monotonous Cu. In conclusion, it is reliable to study the Lewis acidity promoted activity of Cu-MOFs by regulating the ligands with different electron-withdrawing groups towards nitrate to ammonia conversion.

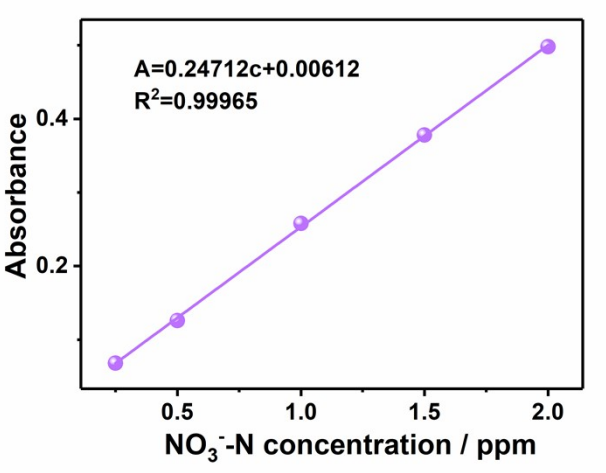

Figure S19 Calibration curves of nitrate-N with good linearity.

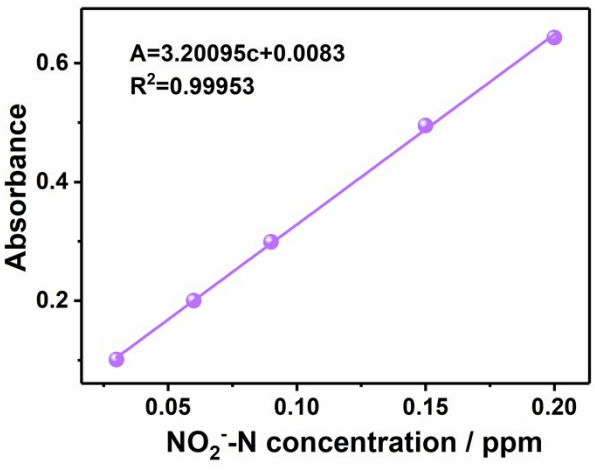

Figure S20 Calibration curves of nitrite-N with good linearity.

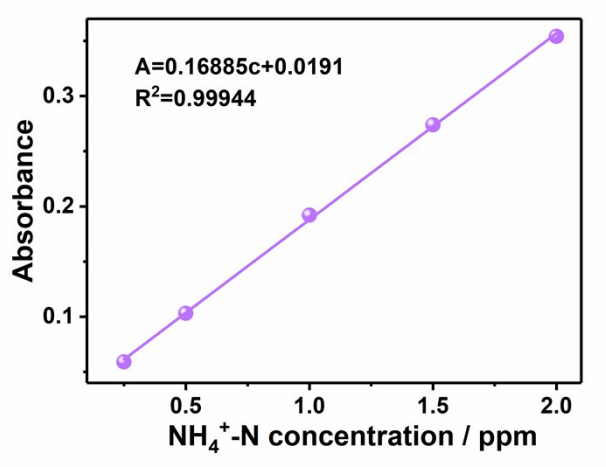

Figure S21 Calibration curves of ammonium-N with good linearity.

Table S1. Comparison of electrochemical nitrate reduction performance with recently published electrocatalyst.

Catalysts	NH_3 Faradaic efficiency	NH_3 yield rate	Potential (V vs. RHE)	Electrolyte	Ref.
Cu-incorporated PTCDA	~77%	0.026 $mmol \cdot h^{-1} \cdot cm^{-2}$	-0.4 V	50 ppm $NaNO_3$-N, 0.1 mM PBS, 0.5 M Na_2SO_4	1
Cu/Cu_2O NWAs	95.8%	0.245 $mmol \cdot h^{-1} \cdot cm^{-2}$	-0.85 V	200 ppm $NaNO_3$-N, 0.5 M Na_2SO_4	2
Fe SAC	~75%	0.308 $mmol \cdot h^{-1} \cdot mg^{-1}$	−0.66 V	50 ppm $NaNO_3$-N, 0.5 M Na_2SO_4	3
TiO_2	66.3%	0.024 $mmol \cdot h^{-1} \cdot mg^{-1}$	-0.94 V	50 ppm $NaNO_3$-N, 0.5 M Na_2SO_4	4
TiO_{2-x}	85.0%	0.045 $mmol \cdot h^{-1} \cdot mg^{-1}$	-0.94 V	50 ppm $NaNO_3$-N, 0.5 M Na_2SO_4	4

Pd-doped TiO_2 nanorod arrays	92.1%	0.065 $mmol \cdot h^{-1} \cdot mg^{-1}$	-0.7 V	0.25 M $LiNO_3$, 1 M LiCl	5
Cu_2O	60.0%	0.035 $mmol \cdot h^{-1} \cdot mg^{-1}$	-0.58 V	50 ppm $NaNO_3$-N, 0.5 M Na_2SO_4	6
Plasma treated Cu_2O	89.5%	0.083 $mmol \cdot h^{-1} \cdot mg^{-1}$	-0.58 V	50 ppm $NaNO_3$-N, 0.5 M Na_2SO_4	6
CuCl-TiO_2/MXene	95.6 %	0.107 $mmol \cdot h^{-1} \cdot cm^{-2}$	-1 V	100 ppm KNO_3-N, 0.5 M K_2SO_4	7
$Cu_3(BTC)_2$@HsGDY nanorod arrays	90.2%	0.265 mmol h^{-1} cm^{-2}	-0.7 V	200 ppm KNO_3-N, 0.5 M Na_2SO_4	This work
Cu(BDC)@HsGDY nanorod arrays	86.4%	0.185 mmol h^{-1} cm^{-2}	-0.6 V	200 ppm KNO_3-N, 0.5 M Na_2SO_4	This work
Cu(BDC-NH_2) @HsGDY nanorod arrays	85.3%	0.225 mmol h^{-1} cm^{-2}	-0.6 V	200 ppm KNO_3-N, 0.5 M Na_2SO_4	This work

REFERENCES

1. G. F. Chen, Y. Yuan, H. Jiang, S. Y. Ren, L. X. Ding, L. Ma, T. Wu, J. Lu, H. Wang, *Nat. Energy,* 2020, **5**, 605–613

2. Y. Wang, W. Zhou, R. Jia, Y. Yu and B. Zhang, *Angew. Chem. Int. Ed.,* 2020, **132**, 5388–5392.

3. Z. Y. Wu, M. Karamad, X. Yong, Q. Huang, D. A. Cullen, P. Zhu, C. Xia, Q. Xiao, M. Shakouri, F. Y. Chen, J. Y. (Timothy) Kim, Y. Xia, K. Heck, Y. Hu, M. S. Wong, Q. Gates, I. Li, S. Siahrostami and H. Wang, *Nat. Commun*., 2021, **12**, 1–10.

4. R. Jia, Y. Wang, C. Wang, Y. Ling, Y. Yu and B. Zhang, *ACS Catal*., 2020**, 10**, 3533–3540.

5. Y. Guo, R. Zhang, S. Zhang, Y. Zhao, Q. Yang, Z. Huang, B. Dong and C. Zhi, *Energy Environ. Sci*., 2021, **14**, 3938–3944.

6. Z. Gong, W. Zhong, Z. He, Q. Liu, H. Chen, D. Zhou, N. Zhang, X. Kang and Y. Chen, *Appl. Catal. B,* 2021, 121021

7. A. W. Sun, H. Ji, L. Li and H. Zhang, *Angew. Chem. Int. Ed*., 2021, **60**, 22933–22939.